Single Nanoparticle Plasmonic Electro-Optic Modulator Based on MoS_2 Monolayers

Bowen Li [†,§], Shuai Zu[†,§], Jiadong Zhou[‡], Qiao Jiang[†], Bowen Du[†], Hangyong Shan[†], Yang Luo[†], Zheng Liu[‡], Xing Zhu[†], and Zheyu Fang[†,*]

[†]School of Physics, State Key Lab for Mesoscopic Physics, Academy for Advanced Interdisciplinary Studies, Peking University, Beijing 100871, China.

[‡]Center for Programmable Materials, School of Electrical and Electronic Engineering, Nanyang Technology University, Singapore 639798.

[*]E-mail: zhyfang@pku.edu.cn

Contents

time-resolved reflectance spectra.

Figure S8. The schematic flowchart illustrating the fabrication process of the heptamer reversible display device.

Figure S9. The U-shaped electro-optic display device and its far-field emission.

Figure S10. The curves of the direct multiplication of the MoS_2 reflectivity at different gate voltages in Figure 2 (a,b) and the Au nanoparticle scattering intensity in Figure 1 (c).

Table S1. The detailed parameter values for the oscillator model calculation.

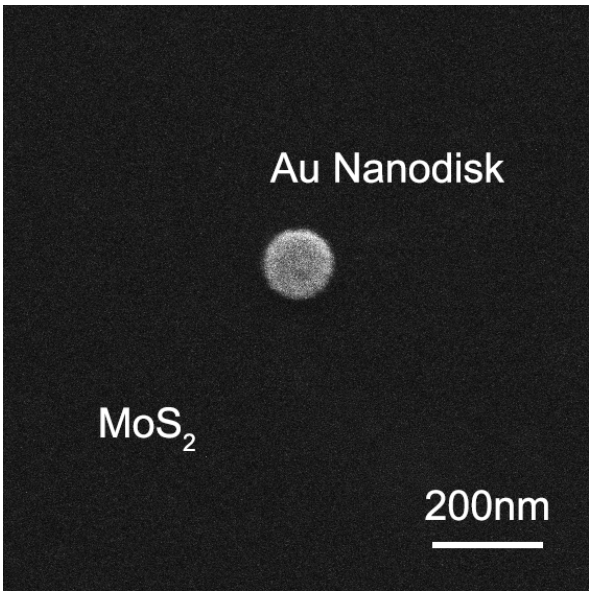

Figure S1. The SEM image of Au disk with radius of 60 nm that patterned on the MoS_2 monolayers.

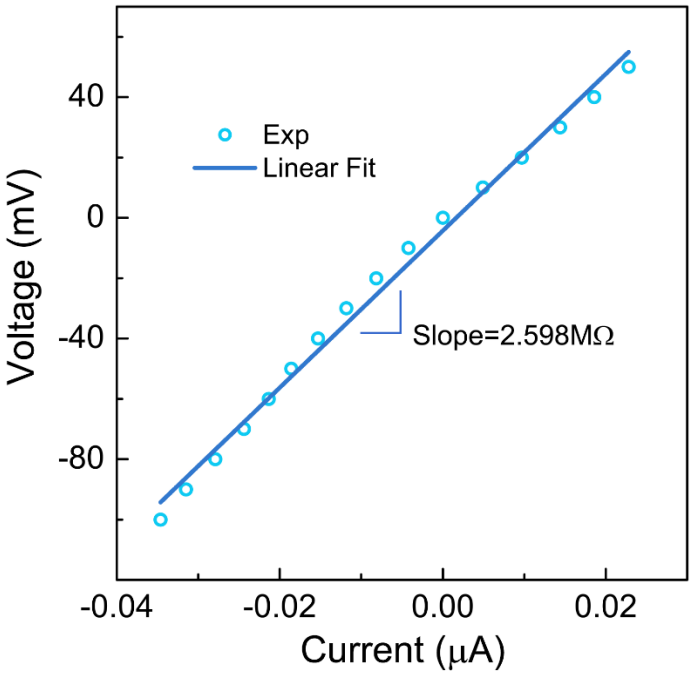

Figure S2. The *I-V* curve that measured between the MoS_2 monolayers and the fabricated electrodes. By calculating the slope of the fitting line, we can obtain the contact resistance is about 2.598 MΩ, which shows a fine Ohmic contact.

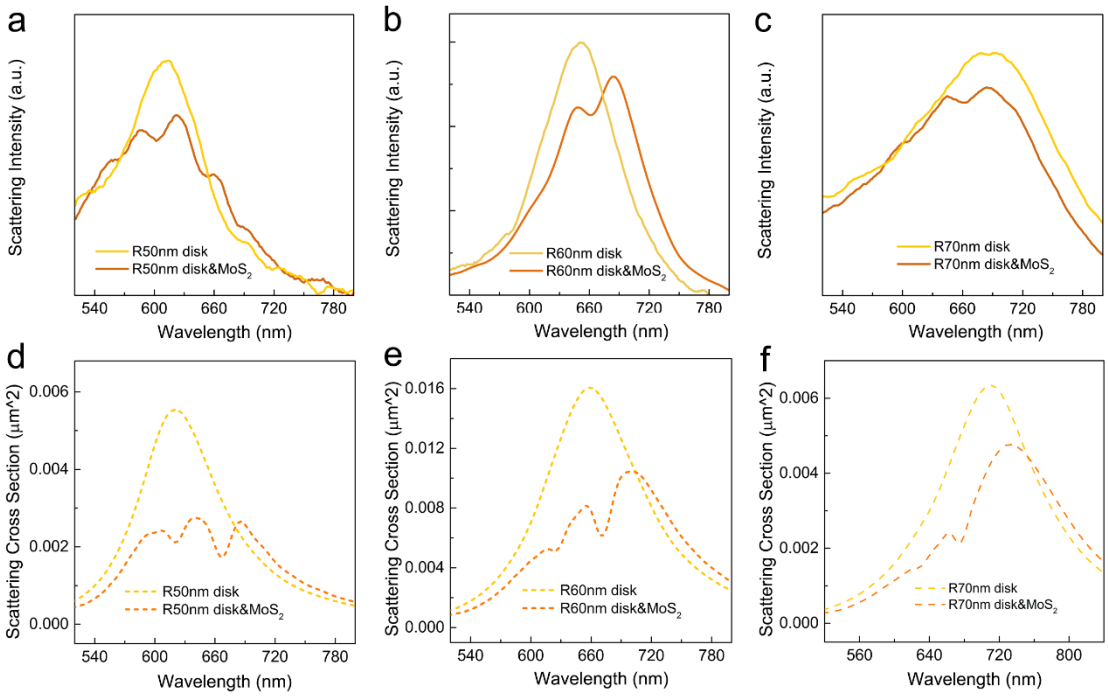

Figure S3. The experimental and FDTD simulated scattering spectra of MoS_2-Au hybrid structure with different sized Au disk. (a-c) Experimental scattering spectra of MoS_2-Au hybrid structure with Au nanodisk radius as (a) 50 nm, (b) 60 nm and (c) 70

nm. (d-f) The FDTD simulation scattering cross section of MoS_2-Au hybrid structure with the same Au nanodisk size as (a-c).

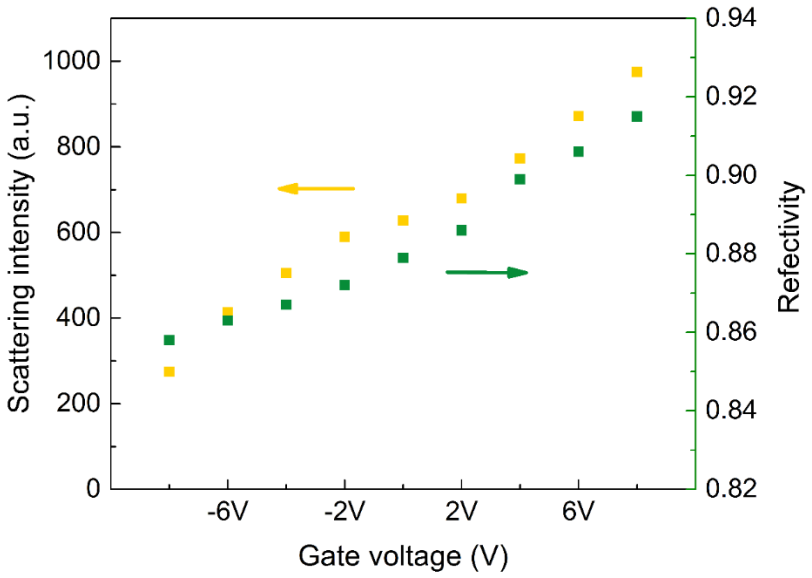

Figure S4: The variation of reflectivity and scattering dip as a function of the applied gate voltages. With the gate voltage increased from -8V to +8V, the reflectivity increases and the absorption of MoS_2 decreases. The scattering dip of Au/MoS_2 hybrids shows the similar tendency because the Fano resonane arises from plasmon-exciton coupling

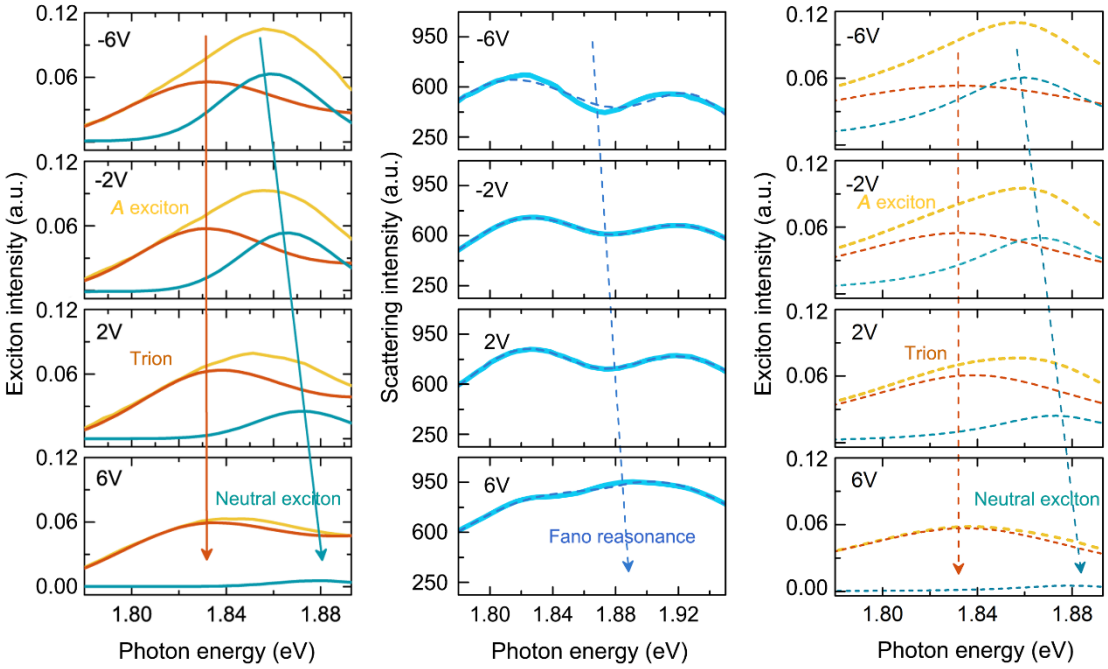

Figure S5. (a) Experimental measured MoS_2 *A* exciton intensity in the energy range of 1.78 eV to 1.9 eV under gate voltages of -6, -2, 2 and 6V. The solid arrows represent the trend of the energy evolution of the neutral exciton and trion, respectively. (b) Measured (solid line) and calculated (dashed line) scattering spectra of Fano resonance in the range of 1.78eV to 1.95 eV under the same gate voltage as (a). (c) The calculated MoS_2 *A* exciton intensity and its corresponding neutral exciton and trion contributions.

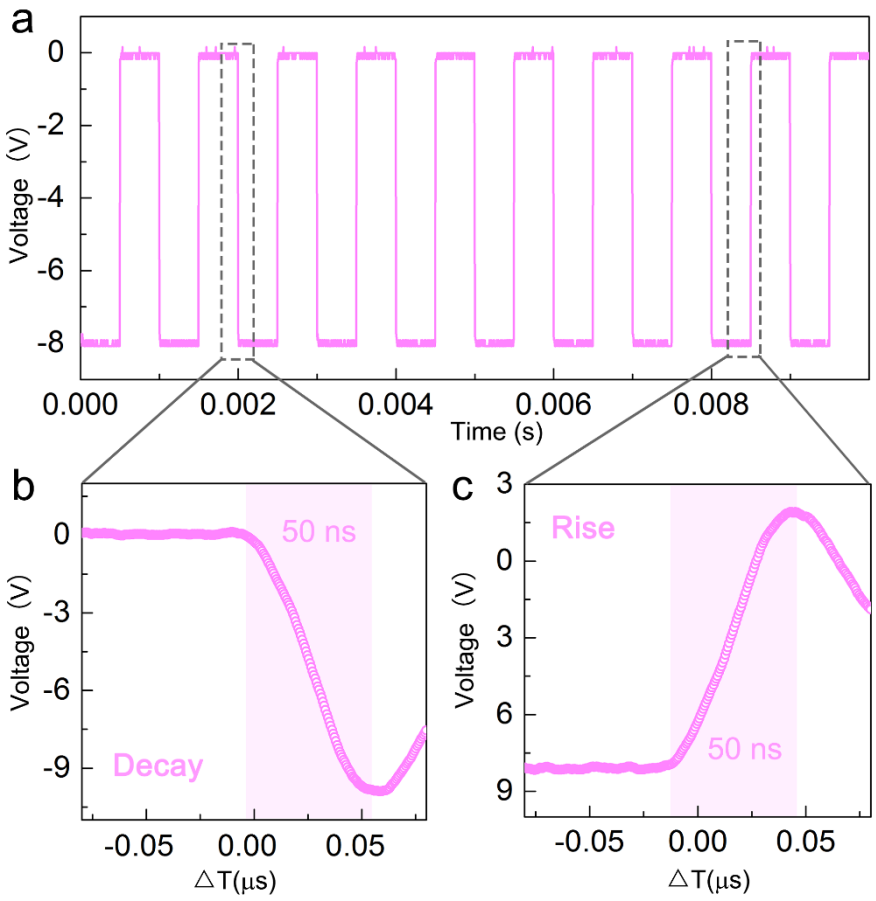

Figure S6. (a) The voltage variation of our device by applying a fast pulse train (-8V) with period of 1 ms and 50% duty cycle. (b) Rise and (c) decay region of the electric response of MoS_2 monolayers, which shows the response time is about 50 ns, which shows the same electric response compared with the positive pulse train case.

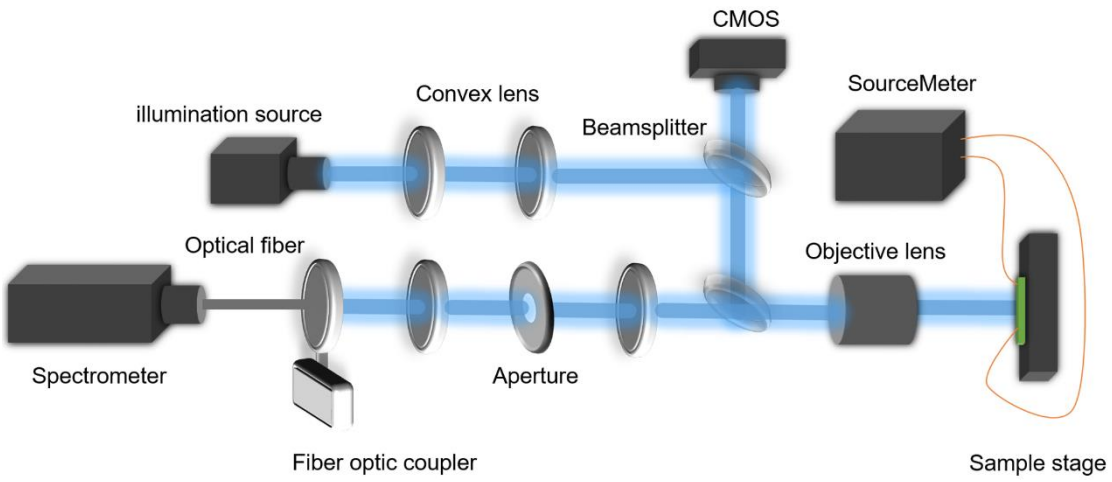

Figure S7. The schematic illustration of the home-built optical system to measure

time-resolved reflectance spectra. The White light from fiber optic illumination system was focused to illuminate the sample, then the generated signal was reflected and divided into two beams *via* beam-splitter. One was collected by a CMOS (DCC1545C-HQ, Thorlabs Co.) to form microscopic imaging, and another was detected by spectrometer (Acton SP2500, Princeton Instruments Co.) after efficiently coupled by a fiber optic coupler. The sourcemeter is connected to the sample for bias control.

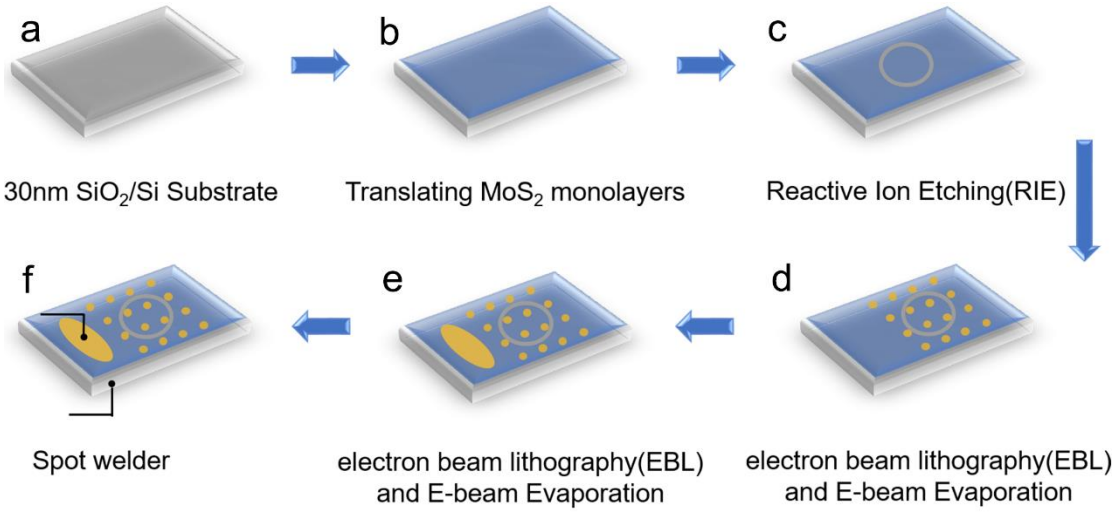

Figure S8. The schematic flowchart illustrating the fabrication process of the heptamer reversible display device. (a) The 30nm SiO_2/Si substrate was prepared by using the ultrasonic cleaning. (b) Translating MoS_2 monolayers on the prepared 30nm SiO_2/Si substrate by using the polymethylmethacrylate (PMMA) nanotransfer method. (c) A portion of the MoS_2 was removed by the reactive ion etching (RIE) to form a heptamer pattern. (d) The Au nanodisks with radius of 60 nm and period of 1 μm were fabricated as a rectangular array on the MoS_2 monolayers by EBL and E-beam Evaporation. (e) The Au electrode was also manufactured by EBL and E-beam Evaporation. (f) By using the spot welder，the Au electrodes were connected to external circuit to realize bias control.

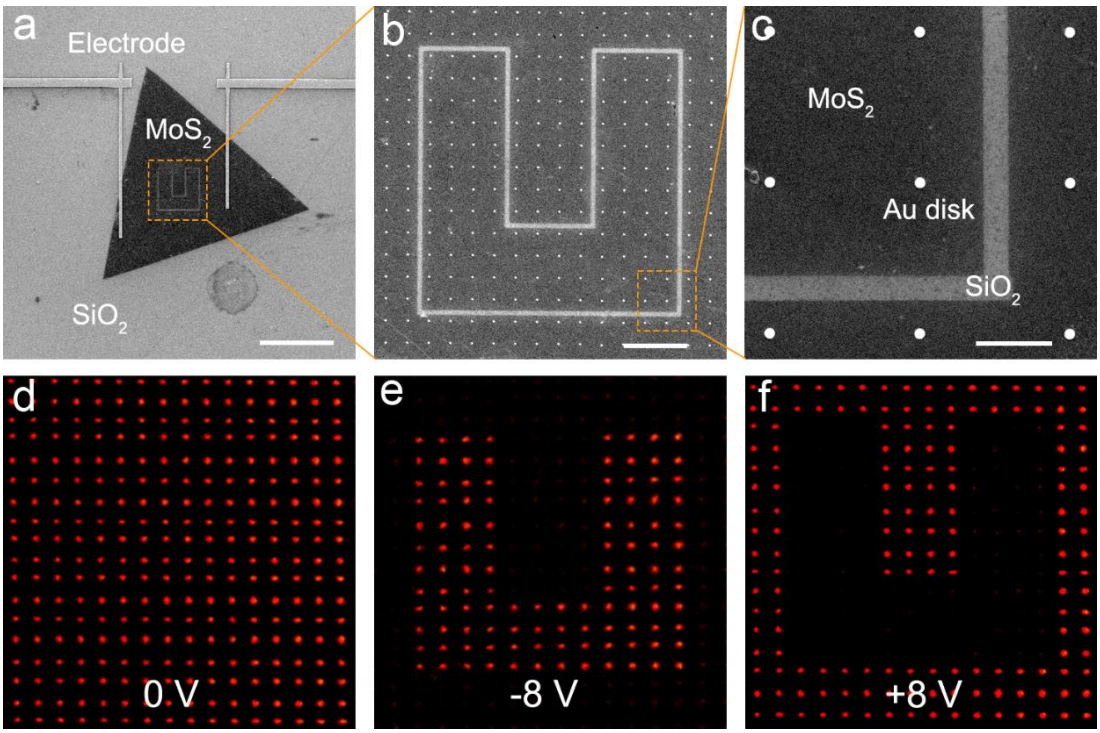

Figure S9. (a-c) SEM images of the fabricated electro-optic display device with different zoom-in scales. A partial of the MoS_2 monolayers was removed to form a U-shape pattern. The scale bars: 20 μm, 6 μm and 1 μm. (d-f) The far-field scattering images with different gate voltage applied, (d) as V_g=0V, the U-shape pattern is invisible and hided in the background; (e) as V_g=-8V, the 'U' appears and become a convex image; (f) as V_g=+8V, the 'U' pattern turned to be a concave one with the background intensity subtracted.

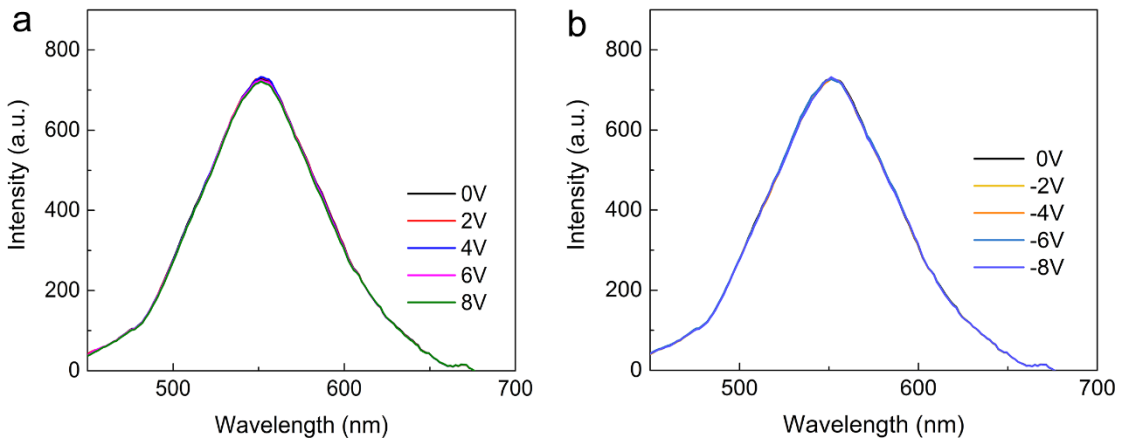

Figure S10. The curves show the direct multiplication of the MoS_2 reflectivity at different gate voltages in Figure 2 (a,b) and the Au nanoparticle scattering intensity in

Figure 1 (c), which have significant difference from the Fano-resonance curves in Figure 2 (c,d).

Gate Voltage (V)	a_1	ω_{LSP}	γ_{LSP}	a_2	ω_{A_0}	γ_{A_0}	a_3	ω_{A^-}	γ_{A^-}	g_1	g_2
8	9.96459	1.91381	0.16931	-0.15535	1.85719	0.06598	-0.29424	1.83616	0.13919	-0.01109	-0.10502
6	8.21540	1.90225	0.08941	-0.17881	1.86001	0.07813	-0.38391	1.83758	0.18121	-0.01322	-0.21606
4	12.33834	1.90552	0.20565	-0.16375	1.86258	0.07651	-0.27577	1.83742	0.12414	-7.27E-04	-0.08476
2	12.46203	1.90971	0.20442	-0.14573	1.86672	0.06946	-0.2757	1.83471	0.12846	-0.00732	-0.0715
0	14.93186	1.90298	0.25421	-0.10178	1.86964	0.06331	-0.27496	1.84088	0.11788	0.00109	-0.06169
-2	12.81764	1.91128	0.19916	-0.09702	1.87299	0.06633	-0.29641	1.84071	0.13067	-4.58E-04	-0.08346
-4	13.7988	1.91544	0.20868	-0.07117	1.87493	0.06468	-0.34561	1.84201	0.15606	3.68E-04	-0.10082
-6	15.92093	1.90475	0.26886	-0.03542	1.87907	0.05241	-0.31139	1.83765	0.14231	6.78E-04	-0.03477
-8	17.39762	1.89774	0.29301	-0.00899	1.8876	0.03551	-0.22917	1.83928	0.10923	3.58E-04	-0.01823

Table S1. The detailed parameter values for the LSPR, neutral exciton, trion and coupling strength as obtained from the fitting curve of Fig. 3b, where ω_{LSP}, ω_{A0}, ω_{A-}, and γ_{LSP}, γ_{A0}, γ_{A-} are the resonance frequencies and damping constants for the LSP, neutral exciton (A_0) and trion (A^-). a_1, a_2 and a_3 are the oscillation amplitudes of the harmonic external force. g_1 and g_2 are the real coupling constants for the LSP-neutral exciton coupling and LSP-trion coupling, respectively.